Wind and Structures, Vol. 11, No. 1 (2008) 35-50
DOI: http://dx.doi.org/10.12989/was.2008.11.1.035

Modeling of wind and temperature effects on modal frequencies and analysis of relative strength of effect

H. F. Zhou†, Y. Q. Ni‡, and J. M. Ko‡†

Department of Civil and Structural Engineering, The Hong Kong Polytechnic University, Hung Hom, Kowloon, Hong Kong

K. Y. Wong‡‡

Bridges and Structures Division, Highways Department, The Hong Kong SAR Government, Hong Kong

(Received August 21, 2007, Accepted January 24, 2008)

Abstract. Wind and temperature have been shown to be the critical sources causing changes in the modal properties of large-scale bridges. While the individual effects of wind and temperature on modal variability have been widely studied, the investigation about the effects of multiple environmental factors on structural modal properties was scarcely reported. This paper addresses the modeling of the simultaneous effects of wind and temperature on the modal frequencies of an instrumented cable-stayed bridge. Making use of the long-term monitoring data from anemometers, temperature sensors and accelerometers, a neural network model is formulated to correlate the modal frequency of each vibration mode with wind speed and temperature simultaneously. Research efforts have been made on enhancing the prediction capability of the neural network model through optimal selection of the number of hidden nodes and an analysis of relative strength of effect (RSE) for input reconstruction. The generalization performance of the formulated model is verified with a set of new testing data that have not been used in formulating the model. It is shown that using the significant components of wind speeds and temperatures rather than the whole measurement components as input to neural network can enhance the prediction capability. For the fundamental mode of the bridge investigated, wind and temperature together apply an overall negative action on the modal frequency, and the change in wind condition contributes less to the modal variability than the change in temperature.

Keywords: modal variability; environmental effect; wind; temperature; relative strength of effect (RSE); neural network; cable-stayed bridge.

1. Introduction

Vibration-based damage detection techniques constitute the fastest growing aspect in the field of structural health monitoring. This kind of techniques uses the measured changes in dynamic

† PhD, Research Associate, E-mail: cehfzhou@polyu.edu.hk
‡ PhD, Associate Professor, Corresponding Author, E-mail: ceyqni@polyu.edu.hk
‡† PhD, Chair Professor, E-mail: cejmko@inet.polyu.edu.hk
‡‡ PhD, Senior Engineer, E-mail: sebh.bstr@hyd.gov.hk

characteristics (mainly modal parameters) to evaluate changes in physical properties that may indicate structural damage or deterioration. In reality, however, civil engineering structures are subject to varying environmental and operational conditions such as wind, temperature, traffic, humidity and solar radiation. These environmental effects also cause changes in modal parameters which may mask the changes caused by structural damage and result in false-positive or false-negative damage diagnosis. It is of paramount importance to formulate the correlation model between modal properties and environmental factors for reliable performance of vibration-based damage detection methods. When such a correlation model is available, the environmental effects in damage detection can be eliminated or reduced by normalizing the measured modal properties before and after structural damage to an identical reference status of environmental factors with the help of the correlation model (Kim, *et al*. 2004, Olson, *et al*. 2005, Wenzel, *et al*. 2005, Kim, *et al*. 2007, Sohn 2007, Zhou, *et al*. 2007).

The previous studies through field measurements and laboratory experiments indicate that temperature accounts for changes in modal frequencies by up to 6% for bridge structures (Robert and Pearson 1996, Abdel Wahab and De Roeck 1997, Cornwell, *et al*. 1999, Alampalli 2000, Lloyd, *et al*. 2000, Rohrmann, *et al*. 2000, Ko, *et al*. 2003, Kim, *et al*. 2004, Xia, *et al*. 2006). It has also been shown that wind is a major contributory to changes in the modal properties of long-span bridges because of the response-amplitude-dependent modal properties and the aeroelastic coupling between wind and bridge (Abe, *et al*. 2000, Mahmoud, *et al*. 2001, Link, *et al*. 2002), whereas vehicle mass has only little influence on the modal properties of large-scale bridges (Kim, *et al*. 2001, De Reock and Maeck 2002, Zhang, *et al*. 2002). As a result, wind and temperature are two main sources causing modal variability in long-span bridges. Research efforts have been made to establish the correlation models between modal frequencies and environmental factors (Sohn, *et al*. 1999, Peeters and De Roeck 2001, Hua, *et al*. 2007). In all the previous studies, only one kind of environmental factor was observed and accounted for while neglecting the effects of other environmental factors. In fact, however, different environmental factors contribute simultaneous effects on the modal variability of a bridge structure.

This paper presents a study on the modeling of the simultaneous effects of wind and temperature on modal frequencies by taking the cable-stayed Ting Kau Bridge as a paradigm. The Ting Kau Bridge in Hong Kong was instrumented with a long-term structural health monitoring system in 1998. With the acquired wind, temperature and vibration data under different wind conditions (including several typhoon events) and temperature conditions, a correlation model is formulated by means of the neural network technique for mapping between the two environmental factors (wind and temperature) and the modal frequency for each mode. As it is aimed to predict the environment-caused modal variability in damage detection, research efforts have been made to enhance the prediction capability of the formulated correlation model. First, the number of hidden nodes of the neural network model is optimized with this target by applying the early stopping technique in consideration of training, validation and testing stages. Then the relative strength of effect (RSE) of the input components is analyzed through evaluating the partial derivatives of the neural network output with respect to its input. Significant input components are selected by leaving out those with small RSEs. The neural network model is then re-configured by using only the significant input components with the aim to eliminate the multicolinearity and further enhance the prediction capability.

2. Theoretical background

2.1. Modeling using neural network technique

Artificial neural networks have been shown to be a powerful mathematical tool for pattern recognition, classification and prediction. They generalize the knowledge implicit in the training samples and become capable of providing solutions to new situations. In this study, a back-propagation neural network (BPNN) model with its input being the environmental factors (wind speed and temperature) and its output being the modal frequency of a specific mode will be formulated using long-term monitoring data from a structure. Consider an m-layer BPNN as shown in Fig. 1, in which the input to the node i in the layer l is

$$x^l(i) = \sum_{j=1}^{S^{l-1}} w^l(i,j) y^{l-1}(j) + b^l(i), \quad l = 1, 2, \cdots, m \tag{1}$$

where $w^l(i,j)$ is the weight connecting the node i in the layer l with the node j in the layer $l-1$; $y^{l-1}(j)$ the output of the node j in the layer $l-1$; $b^l(i)$ the bias of the node i in the layer l; and S^{l-1} the number of nodes in the layer $l-1$. The output of the node i is

$$y^l(i) = f^l(x^l(i)) \tag{2}$$

where f^l is the transfer function in the layer l.

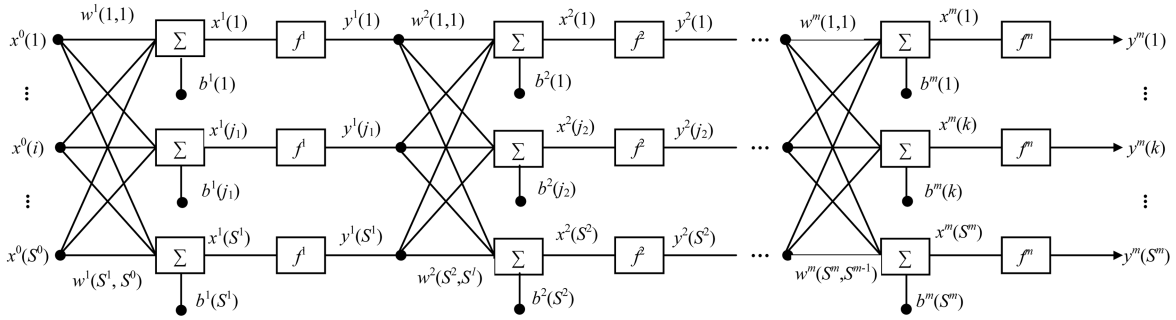

Fig. 1 An m-layer BPNN

It has been proven that a two-layer BPNN with biases, a sigmoid transfer function for the hidden layer, and a linear transfer function for the output layer is capable of approximating any function with a finite number of discontinuities to an arbitrary degree of precision (Cybenko 1989). Such a BPNN is therefore employed in the present study. It is known that taking into consideration thermal inertia effect can provide a more accurate representation of the temperature-frequency correlation when continuous measurement data are available (Peeters and De Roeck 2001, Hua, *et al*. 2007). However, the long-term measurement data from an on-line monitoring system are usually discontinuous because of the existence of an automatic trigger system and abnormal signals. Due to this reason and to facilitate the combination with damage detection methods, the BPNN is

configured herein for the correlation between instant modal frequency and instant environmental condition. As a result, the number of input nodes is equal to the number of available wind and temperature measurement components in a structure, while the output layer has only one node that represents the modal frequency at a specific mode. As shown later, the number of nodes in the hidden layer is determined so as to have good prediction capability of the formulated model.

In regard to the application for damage detection, we are more concerned about the prediction (generalization) capability of the formulated correlation model than its reproduction (simulation) capability. Several regularization techniques to enhance the generalization capability of neural networks are available, which include the AIC/FPE technique (Alippi 1996, Ljung 1999), the early stopping technique (Morgan and Bourlard 1990, Amari, *et al*. 1997), and the Bayesian regularization technique (Mackay 1992, Foresee and Hagan 1998). These regularization techniques also help release basic rules of thumb that relate the total number of trainable weights to the number of training data. On the basis of a comparative study of these procedures (Ni, *et al*. 2007), the early stopping technique is employed herein to attain an optimized neural network configuration. For doing so, the data available for model formulation are divided into three subsets, i.e., training, validation, and testing sets. The weights and biases of the neural network are optimized with the training set while the progression of the optimization process is regulated by the performance of the resulting network on the validation set. The error on the validation set is monitored during the training process. It will normally decrease during the initial phase of training, as does the error on the training set. However, when the neural network becomes overfitting, the error on the validation set will typically begin to rise. When the validation error increases for a specific number of iterations, the training is stopped and the weights and biases at the minimum of the validation error are returned. The optimal model is taken as the one which generates the minimal validation error. By repeating this process for different numbers of hidden nodes, a family of optimal models is obtained and the best BPNN model that achieves the global minimum of the validation error is picked out. The prediction capability of such formulated BPNN model will be verified using the testing set that has not been used in formulating the model.

2.2. Analysis of relative strength of effect (RSE)

Since both wind and temperature account for modal variability, it is desirable to quantitatively understand their RSEs on the variation in modal properties. Likewise, when a long-span bridge is instrumented with a monitoring system, each type of sensors (anemometers, temperature sensors, etc.) are usually deployed at different locations and levels of the bridge. As a result, the data from multiple measurement points may be highly correlated. When the highly correlated data are wholly used for modeling, the resulting correlation model may perform unsatisfactorily in prediction due to the multicolinearity (Rencher 2002). In the present study, the RSE analysis is carried out to identify the significant components of wind and temperature measurement data, which will be used to re-configure the neural network model for improvement of its prediction capability. Another well-known approach for the same purpose is the principal component analysis (PCA) (Jolliffe 2002). Compared with PCA, the RSE analysis adopted in the present study has the advantage that it is capable of quantifying the RSEs of various environmental components. In addition, the significant components identified by the RSE analysis possess physical meanings whereas the features extracted by PCA do not. The identified significant components also provide an instruction on the optimal placement of sensors.

The RSE analysis for a correlation model in terms of neural network aims to identify the significance of each cause factor (input) on the effect factors (output). It can be conducted by evaluating the partial derivatives of output components of the neural network with respect to its input components at the training session (Yang and Zhang 1997). For the BPNN shown in Fig. 1, the partial derivative of the ith output with respect to the ith input can be expressed as

$$\frac{\partial y^m(k)}{\partial x^0(i)} = \sum_{j_{m-1}=1}^{S^{m-1}} \sum_{j_{m-2}=1}^{S^{m-2}} \cdots \sum_{j_1=1}^{S^1} w^m_{k,j_{m-1}} G(x^m(k)) w^{m-1}_{j_{m-1},j_{m-2}} G(x^{m-1}(j_{m-1})) \cdots w^1_{j_1,i} G(x^1(j_1)) \quad (3)$$

where $G(\cdot)$ is the differentiation of the output of the considered neuron to its input. The commonly utilized transfer functions, such as log-sigmoid, tan-sigmoid, and linear functions are differentiable and thus Eq. (3) always exists. For the network configuration employed in the present study (a tan-sigmoid hidden layer and a linear output layer), Eq. (3) is elaborated as

$$\frac{\partial y^2(k)}{\partial x^0(i)} = \sum_{j_1=1}^{S^1} w^2_{k,j_1} \frac{4\exp(-2x^1(j_1))}{(1+\exp(-2x^1(j_1)))^2} w^1_{j_1,i} \quad (4)$$

The RSE of the ith input on the kth output, RSE_{ki}, is obtained by normalizing the partial derivative $\frac{\partial y^m(k)}{\partial x^0(i)}$ to a constant which controls the maximum absolute value of RSE_{ki} to unity, i.e.,

$$RSE_{ki} = \frac{1}{C}\left(\frac{\partial y^m(k)}{\partial x^0(i)}\right), \; C = \max\{|RSE_{ki}|, \; i = 1, 2, \cdots, S^0\} \quad (5)$$

It is obvious that RSE ranges between −1 and 1 for any input variable. The larger the absolute value of RSE, the greater the effect the corresponding input variable has on the output variable. The sign of RSE indicates the direction of influence. The input variable applies a positive action on the output variable when RSE > 0 and a negative action when RSE < 0. A positive action means that the output increases with the increase of the corresponding input, while a negative action means that the output decreases with the increase of the corresponding input. A zero value of RSE implies that the input variable has no influence on the output variable.

3. Instrumented bridge

3.1. Monitoring system

The Ting Kau Bridge, as shown in Fig. 2, is a multi-span cable-stayed bridge with three towers supporting two main spans of 448 m and 475 m respectively and two side spans of 127 m each. A unique feature of the bridge is its arrangement of the three single-leg towers that are strengthened by longitudinal and transverse stabilizing cables. After completing its construction in 1998, the bridge was instrumented with a long-term structural health monitoring system by the Highways Department of the Hong Kong SAR Government (Wong 2004). The system involves more than 230 sensors and accomplishes 24-hour monitoring per day.

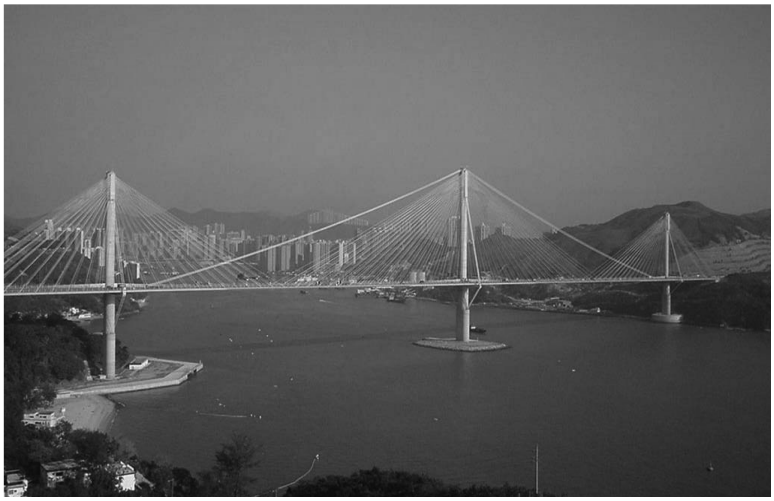

Fig. 2 Ting Kau Bridge

As part of the monitoring system, 7 anemometers have been permanently installed on the bridge to surveil the wind environments, of which four ultrasonic-type anemometers are positioned at the deck level and the other three propeller-type anemometers at the tower top. Likewise, a total of 83 temperature sensors have been installed at different locations of the bridge to measure: (i) steel-girder temperature, (ii) temperature inside concrete deck, (iii) temperature in tower legs, (iv) temperature in asphalt pavement, and (v) atmosphere temperature. For vibration measurement of the bridge, 24 uni-axial accelerometers, 20 bi-axial accelerometers and 1 tri-axial accelerometer (a total of 67 signal channels) have been installed on the deck of two main spans and two side spans, the longitudinal stabilizing cables, the top of the three towers, and the base of the central tower. Fig. 3 illustrates the deployment locations of anemometers, temperature sensors and accelerometers on the bridge.

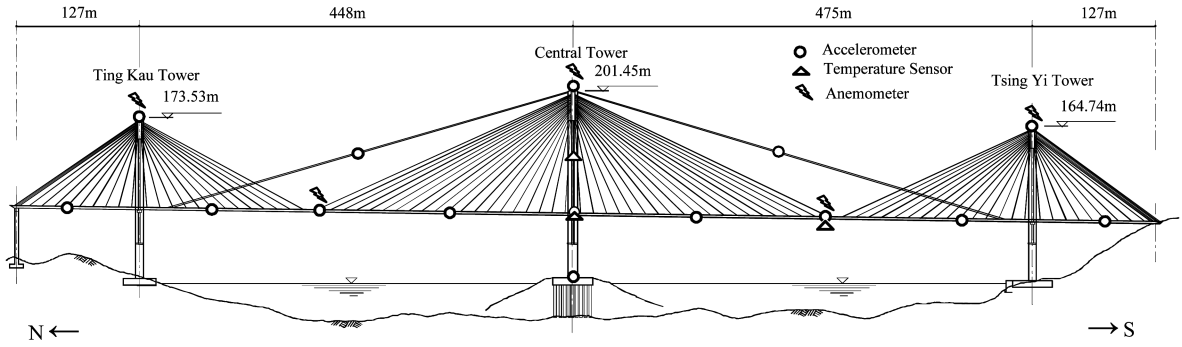

Fig. 3 Deployment locations of anemometers, temperature sensors and accelerometers

3.2. Measurement data

A total of 152-hour monitoring data covering three typhoon events constitute the database for this study. As given in Table 1, the maximum hourly-averaged wind speed measured at the tower top is respectively 14.5, 14.1, and 17.6 m/s during the three typhoon events. To facilitate the data processing,

Table 1 Durations and maximum wind speeds of three typhoon events

Typhoon	Time period of data	Duration (hours)	Maximum wind speed (m/s)
Leo	12:00 of 2 May to 05:00 of 4 May	42	14.5
Maggie	16:00 of 7 June to 08:00 of 9 June	41	14.1
Cam	00:00 of 25 September to 23:00 of 27 September	72	17.6

Table 2 Locations of 20 selected temperature sensors

Number	Category	Location
1	Steel-girder temperature	East side of deck
2		East side of deck
3		West side of deck
4		West side of deck
5	Air temperature	North outer side of central tower at 73 m high
6		South outer side of central tower at 143 m high
7		Under east side of deck
8		Above east side of deck
9	Temperature in tower leg	North inner side of central tower at 73 m high
10		East inner side of central tower at 73 m high
11		South inner side of central tower at 73 m high
12		West inner side of central tower at 73 m high
13	Temperature inside concrete deck panel	East side of deck
14		East side of deck
15		West side of deck
16		West side of deck
17	Temperature in asphalt pavement	East side of deck
18		East side of deck
19		West side of deck
20		West side of deck

the wind speed data acquired from the anemometers installed at the same level are averaged to form the mean wind speed at that level. Likewise, four temperature sensors which are deployed at the locations most susceptible to temperature variation are preliminarily selected from each of the five temperature monitoring categories. Consequently a total of 20 temperature sensors, as listed in Table 2, are chosen to provide temperature measurement data for the present study. With the acceleration data acquired from all the 67 accelerometer channels, modal parameters of the bridge were identified at one-hour intervals by using an output-only modal identification program (Ni, *et al*. 2005). The identified modal shapes for the first two modes of the bridge are shown in Fig. 4, in which the legend 'U' denotes the undeflected bridge deck configuration; the legends 'V1' and 'V2' denote the deck vertical modal components at western and eastern edges, respectively; and the

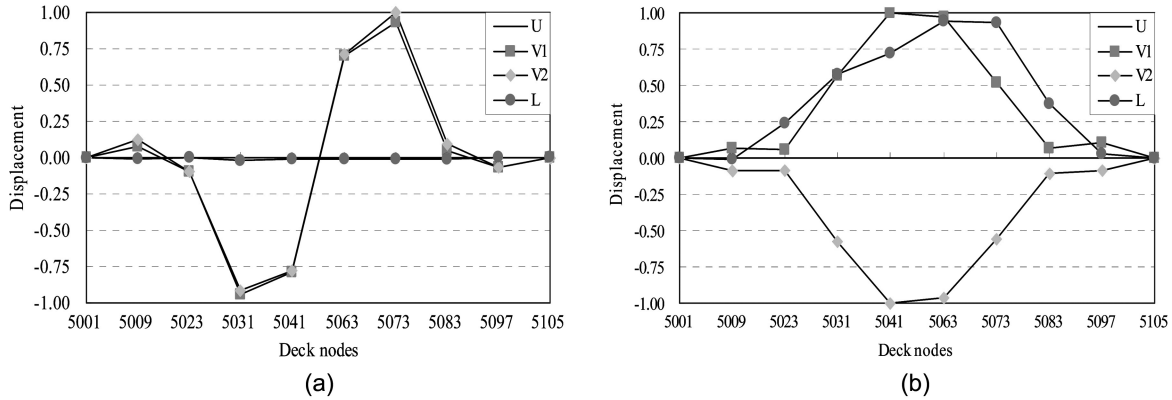

Fig. 4 Identified modal shapes of the bridge: (a) 1st mode; (b) 2nd mode

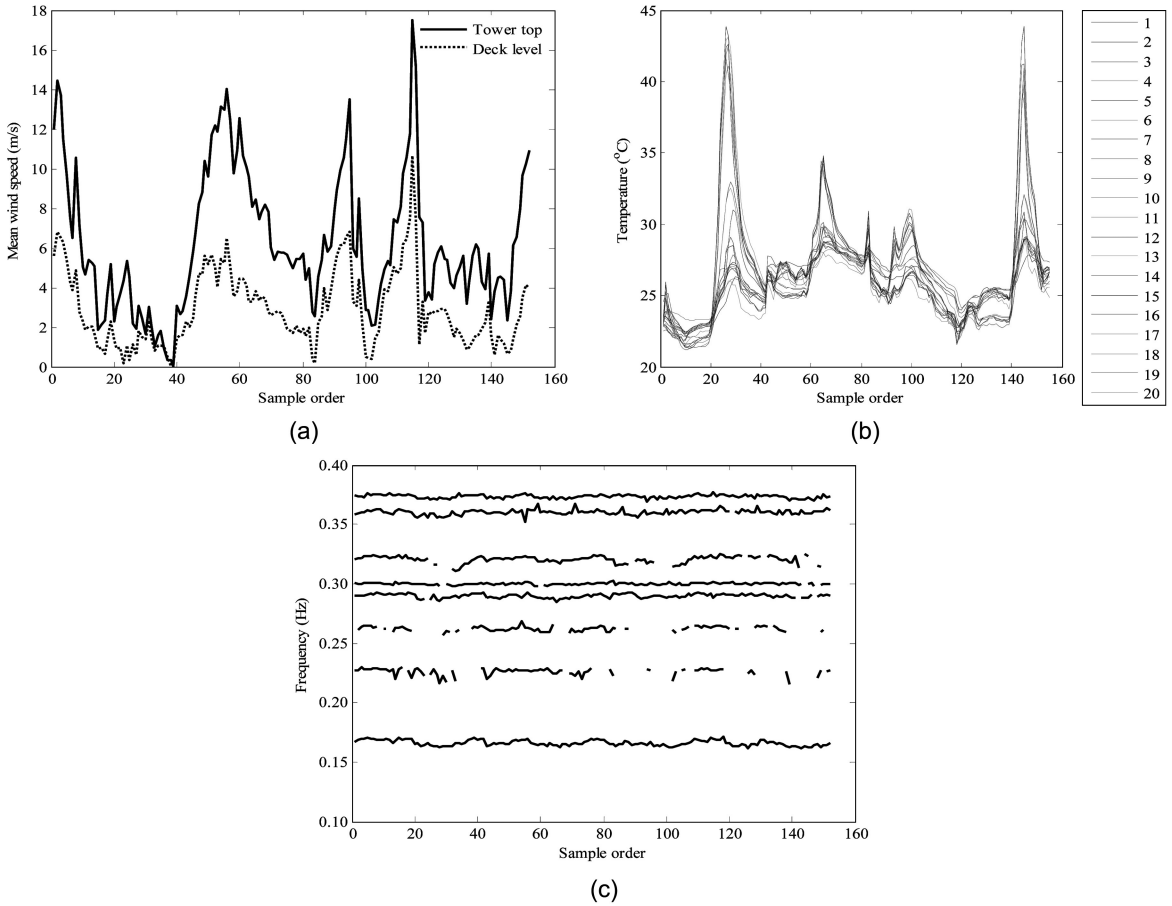

Fig. 5 Sequences of measured mean wind speeds, hourly-averaged temperatures and modal frequencies: (a) Wind speed; (b) Temperature; (c) Modal frequency

legend 'L' denotes the deck lateral modal components at central girder. Fig. 5 illustrates the sequences of the mean wind speeds at the deck level and tower top, the hourly-averaged

temperatures from the 20 sensors, and the measured modal frequencies for the first eight modes. Discontinuity in the modal frequency sequences as shown in Fig. 5(c) is due to the failure of modal identification for some time intervals in which the coupled torsional and lateral vibration modes of the bridge were not motivated. As the identified modal frequencies of higher modes are incomplete, the present study focuses on analyzing the effects of wind and temperature on the first modal frequency. It has been reported that wind normally excites the fundamental mode predominantly (Pan, *et al*. 2004, Brownjohn, *et al*. 2005).

4. Development of correlation model

4.1. Model formulation using whole measurement components

The mean wind speeds at the deck level and tower top and the temperatures at the 20 selected locations are first used as input to formulate the neural network model. In this case the number of input nodes is 22 (two wind speed components and 20 temperature components) and the number of output nodes is 1 (modal frequency at a specific mode). To accommodate the early stopping technique, the first half of the 152-hour monitoring data are taken as the training set and the second half of the 152-hour monitoring data are equally divided as the validation and testing sets. As a result, 78 training samples, 39 validation samples and 39 testing samples are discretionarily constituted without overlap. The early stopping technique is then applied to construct a family of optimal BPNNs with various hidden nodes, where the training samples are used to train the neural network while the validation samples are used to monitor the training progression until a minimal validation error is generated for each number of hidden nodes. To find the global minimum of performance function, each BPNN is trained 500 runs with different random initializations of the free parameters using the Levenberg-Marquardt algorithm. Each run is terminated within a maximum epoch of 10,000. Fig. 6 shows the averaged validation errors of the optimal BPNNs for the first mode when the number of hidden nodes n varies from 1 to 40. Here the validation error is represented by the mean square error (MSE) between the target output of the validation data and the predicted output when feeding the validation input data into the BPNN. It is observed that the validation error (MSE) decreases monotonously with the increase of n until it reaches a minimum at

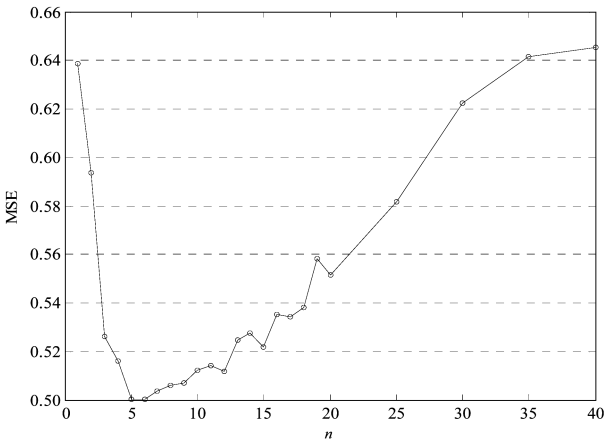

Fig. 6 MSE of validation data versus number of hidden nodes

$n = 5$. As n increases beyond five, the validation error turns to increase on the whole. As a result, the BPNN with five hidden nodes is picked out as the best model. For the simplicity of notation, this BPNN is denoted as NN1 hereafter.

Fig. 7 shows a comparison between the measured modal frequencies and those generated by NN1 for training, validation, and testing data sets at the first mode. To quantitatively evaluate the reproduction (simulation) and prediction (generalization) capabilities, two indices are defined. The first index is the residual

$$e = f_n - f_m \tag{6}$$

where f_n is the modal frequency output generated by the BPNN under the input of training, validation or testing data; f_m is the corresponding target output. The second index is the correlation coefficient which is defined as

$$R = \frac{S_{nm}}{\sqrt{S_{nn}} \cdot \sqrt{S_{mm}}} \tag{7}$$

where S_{nn} is the variance of f_n; S_{mm} the variance of f_m; and S_{nm} the covariance between f_n and f_m.

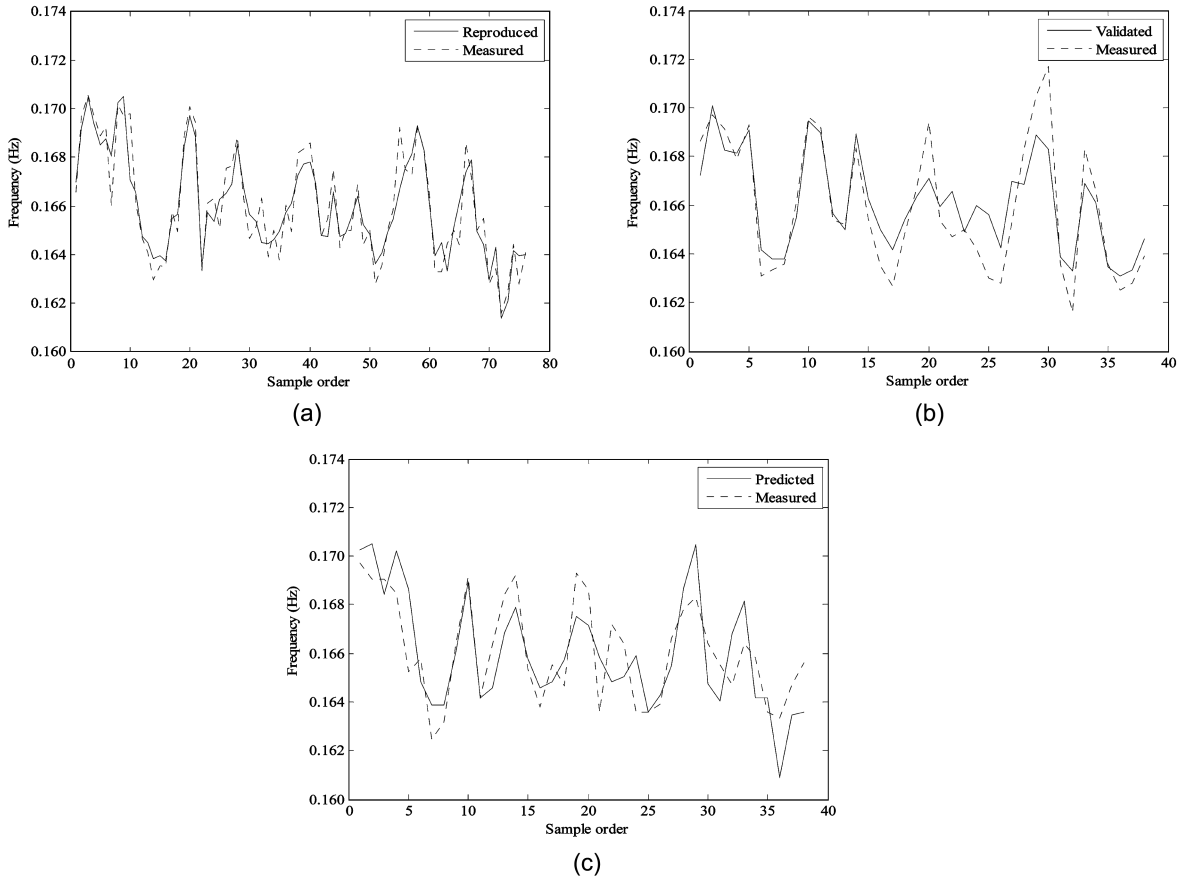

Fig. 7 Comparison between NN1-generated and measured first modal frequencies: (a) Training set; (b) Validation set; (c) Testing set

Table 3 shows the root mean square (RMS) and the standard deviation (SD) of the residuals of NN1-generated modal frequencies. It is seen that both RMS and SD of the residuals for training data are smaller than those for testing data, indicating that the reproduction capability of NN1 is better than its prediction capability. Table 4 shows the correlation coefficients between the NN1-generated and measured modal frequencies. With the larger correlation coefficient for training data than for testing data, the superiority of reproduction capability over prediction capability is evidenced again. An effort to enhance the prediction capability will be made later.

The RSE analysis of NN1 is carried out with training data. Fig. 8 illustrates the RSEs of the 22 input components generated by NN1, where the first 20 components are temperatures and the last two components are wind speeds at the towre top and deck level. It is seen that the 12th input component has the largest absolute value of RSE, which imposes the strongest effect on the first modal frequency among the 22 input components. It applies a negative action on the first modal frequency, i.e., the first modal frequency decreases with the increase of this component. The RSE of the 3rd input component is the smallest (-0.001), which has the least effect on the modal frequency. Besides, the effects of the 8th, 10th, and 21st input components on the first modal frequency are also negligible because their RSEs are nearly zero. With the obtained RSE values, it is obvious that the temperatures affect the modal variability more significantly than the wind speeds. It is also found that the effect of wind speed at the deck level gains dominance over that at the tower top.

Table 3 Statistics of residuals of NN1-generated first modal frequencies

Root mean square (RMS) ($\times 10^{-3}$)			Standard deviation (SD) ($\times 10^{-3}$)		
Training	Validation	Testing	Training	Validation	Testing
0.832	1.234	1.520	0.838	1.239	1.539

Table 4 Correlation coefficients between NN1-generated and measured first modal frequencies

Correlation coefficient		
Training	Validation	Testing
0.930	0.911	0.762

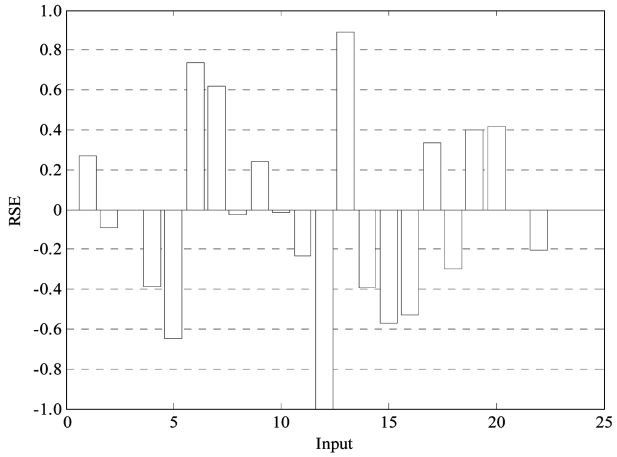

Fig. 8 RSEs of input components generated by NN1

The RSE of wind speed at the tower top (the 21st input component) ranks the last but one. The sum of RSEs for the 22 input components is −0.496, showing an overall negative action of the wind speeds and temperatures on the first modal frequency.

4.2. Model formulation using significant components

Based on the RSE analysis, the significant input components of wind speeds and temperatures can be identified by leaving out those with zero or nearly zero RSEs. According to Fig. 8, the three temperature components (the 3rd, 8th, and 10th components) and the wind speed at the tower top (the 21st component) with small RSEs are considered as insignificant input components, while the other 18 significant input components are used as input to re-configure BPNN. In this case the number of input nodes reduces to 18 and the number of output nodes remains as 1. By applying the early stopping technique in the same way as before, it is obtained that the BPNN with seven hidden nodes achieves a minimal validation error. This BPNN, denoted as NN2, is selected as the best model with the input of significant components.

Fig. 9 shows a comparison between the measured modal frequencies and those generated by NN2

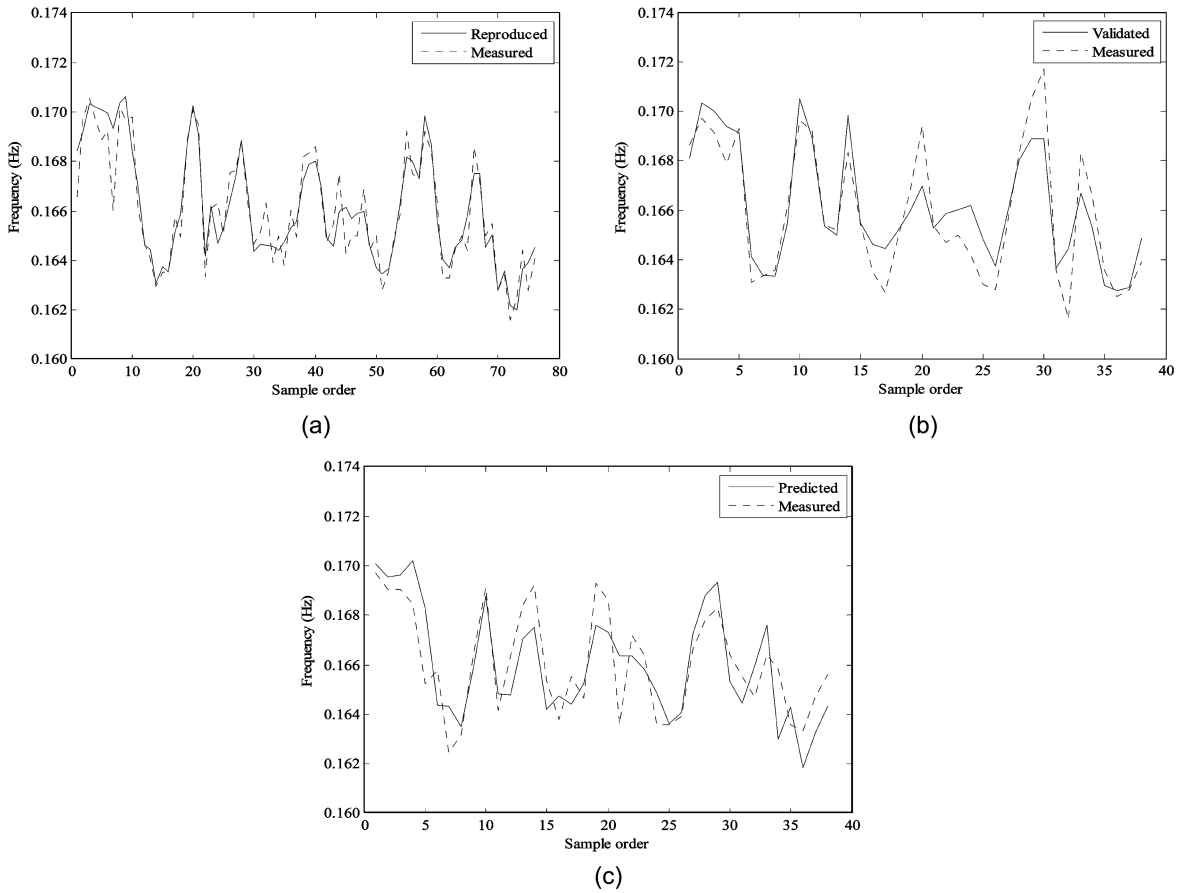

Fig. 9 Comparison between NN2-generated and measured first modal frequencies: (a) Training set; (b) Validation set; (c) Testing set

for training, validation, and testing data sets at the first mode. The root mean square (RMS) and the standard deviation (SD) of the residuals of NN2-generated modal frequencies are summarized in Table 5. By comparing Table 5 (the results of NN2) with Table 3 (the results of NN1), it is found that the RMS and SD of the residuals for training data increase 3.823% and 4.101%, respectively; while those for testing data decrease 10.424% and 10.369%, respectively. It demonstrates that NN2 offers worse reproduction capability but better prediction capability than NN1. Table 6 shows the correlation coefficients between the NN2-generated and measured modal frequencies. It is seen that NN2 achieves comparable correlation coefficients for testing data and for training data. A comparison of Table 6 with Table 4 indicates again the superiority in prediction capability and the inferiority in reproduction capability of NN2 over NN1. Thus, a BPNN model with better prediction capability has been formulated by using the significant input components of wind speeds and temperatures. It is known that the neural network learns in stages, moving from realization of fairly simple to more complex mapping functions. As the training progresses, the neural network model is trying to assign some importance to the least significant input components as well, instead of treating them as a pure noise, which distorts the true output and input mapping. As a result, a better neural network model shall be formulated by discarding the least significant input components from the network input and using the significant input components only.

Fig. 10 shows the RSEs of the significant input components generated by NN2. For the

Table 5 Statistics of residuals of NN2-generated first modal frequencies

Root mean square (RMS) ($\times 10^{-3}$)			Standard deviation (SD) ($\times 10^{-3}$)		
Training	Validation	Testing	Training	Validation	Testing
0.850	1.200	1.335	0.852	1.199	1.352

Table 6 Correlation coefficients between NN2-generated and measured first modal frequencies

Correlation coefficient		
Training	Validation	Testing
0.929	0.900	0.804

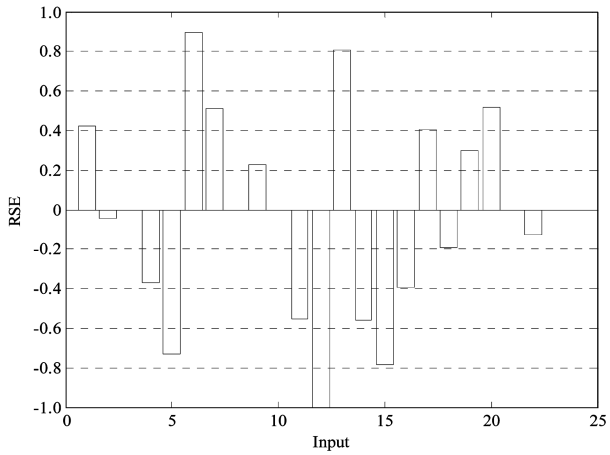

Fig. 10 RSEs of input components generated by NN2

Table 7 Locations of temperature components with large RSE

Component	Category	Location
5th	Air temperature	North outer side of central tower at 73 m high
6th	Air temperature	South outer side of central tower at 143 m high
12th	Concrete temperature	West inner side of central tower at 73 m high
13th	Concrete temperature	East side of deck panel
15th	Concrete temperature	West side of deck panel

convenience of comparison, the insignificant input components, which were left out in formulating the model, are also plotted in this figure with their RSEs equal to zero. The RSEs generated by NN2 coincide well with the RSEs generated by NN1. The dominance of the 12th component remains unchanged. The nature of actions of all the input components in NN2 remains the same as that in NN1. An overall negative effect of the significant components on the first modal frequency is shown again. Table 7 indicates the locations of the temperature components with large RSE. It is found that temperatures at the south and east sides (to the bridge alignment) of the bridge exert positive effects on the first modal frequency; while temperatures at the north and west sides (to the bridge alignment) of the bridge impose negative effects on the first modal frequency. As the alignment of the Ting Kau Bridge is north by west and south by east, the south-east side to the bridge alignment is the sun rise side and the north-west side to the bridge alignment is the sun set side. Hence the temperatures at the sun rise side induce positive effects on the first modal frequency; while the temperatures at the sun set side exert negative effects on the first modal frequency. The implication of this observation deserves further study.

5. Conclusions

In this paper, the simultaneous effects of wind and temperature on the modal frequencies of the cable-stayed Ting Kau Bridge have been investigated. Making use of the long-term monitoring data of wind, temperature and structural dynamic response obtained from the bridge, a neural network model has been developed to correlate the modal frequencies with wind speed and temperature simultaneously. The early stopping technique has been applied to optimize the neural network configuration, and a RSE-analysis-based method has been proposed for constructing appropriate input to the BPNN to enhance its generalization performance. The prediction capability of the formulated neural network model was verified with the testing data which had not been used in training and validating the neural network. For the bridge investigated, the following conclusions are drawn: (i) the wind and temperature together apply an overall negative action on the fundamental modal frequency; (ii) the change in wind speed, even under the action of typhoons, contributes less to the modal variability than the change in temperature; (iii) the wind at the deck level is dominant in affecting the fundamental modal frequency than the wind at the tower top; and (iv) using the significant components of wind speeds and temperatures as input to neural network can enhance the prediction capability.

Acknowledgements

The work described in this paper was supported in part by a grant from the Research Grants

Council of the Hong Kong Special Administrative Region, China (Project No. PolyU 5142/04E) and partially by a grant from the Hong Kong Polytechnic University (Project No. A-PG42). The writers also wish to thank the Hong Kong SAR Government Highways Department for providing support to this research.

References

Abdel Wahab, M. and De Roeck, G. (1997), "Effect of temperature on dynamic system parameters of a highway bridge", *Struct. Eng. Int.*, **7**, 266-270.

Abe, M., Fujino, Y., Yanagihara, M. and Sato, M. (2000), "Monitoring of Hakucho Suspension Bridge by ambient vibration measurement", *Nondestructive Evaluation of Highways, Utilities, and Pipelines IV*, A. E. Aktan and S. R. Gosselin (eds.), SPIE, Bellingham, Washington, USA, **3995**, 237-244.

Alampalli, S. (2000), "Effects of testing, analysis, damage, and environment on modal parameters", *Mechanical Systems and Signal Processing*, **14**, 63-74.

Alippi, C. (1996), "Extending the FPE and the effective number of parameters to neural estimators", *Proceedings of the IEEE International Conference on Neural Networks*, Washington, D.C., USA, **1**, 217-222.

Amari, S., Murata, N., Muller, K. R., Finke, M. and Yang, H. H. (1997), "Asymptotic statistical theory of overtraining and cross-validation", *IEEE Transactions on Neural Networks*, **8**, 985-996.

Brownjohn, J. M. W., Moyo, P., Omenzetter, P. and Chakraborty, S. (2005), "Lessons from monitoring the performance of highway bridges", *Struct. Control Health Monitoring*, **12**, 227-244.

Cornwell, P., Farrar, C. R., Doebling, S. W. and Sohn, H. (1999), "Environmental variability of modal properties", *Experimental Techniques*, **23**, 45-48.

Cybenko, G. (1989), "Approximation by superpositions of a sigmoidal function", *Mathematics of Control, Signals and Systems*, **2**, 303-314.

De Roeck, G. and Maeck, J. (2002), "Influence of traffic on modal properties of bridges", *Proceedings of the 1st European Workshop on Structural Health Monitoring*, D. L. Balageas (ed.), DEStech Publications, Lancaster, Pennsylvania, USA, 989-998.

Foresee, F. D. and Hagan, M. T. (1998), "Gauss-Newton approximation to Bayesian regularization", *Proceedings of the 1997 International Joint Conference on Neural Networks*, IEEE, Piscataway, New Jersey, USA, 1930-1935.

Hua, X. G., Ni, Y. Q., Ko, J. M. and Wong, K. Y. (2007), "Modeling of temperature-frequency correlation using combined principle component analysis and support vector regression technique", *J. Comput. Civil Eng.*, ASCE, **21**, 122-135.

Jolliffe, I. T. (2002), *Principal Component Analysis*, 2nd edition, Springer, New York, USA.

Kim, C. Y., Jung, D. S., Kim, N. S. and Yoon, J. G. (2001), "Effect of vehicle mass on measured dynamic characteristics of bridge from traffic-induced vibration test", *Proceedings of the 19th International Modal Analysis Conference*, SEM, Bethel, Connecticut, USA, 1106-1111.

Kim, J. T., Park, J. H. and Lee, B. J. (2007), "Vibration-based damage monitoring in model plate-girder bridges under uncertain temperature conditions", *Eng. Struct.*, **29**, 1354-1365.

Kim, J. T., Yun, C. B. and Yi, J. H. (2004), "Temperature effects on modal properties and damage detection in plate-girder bridges", *Advanced Smart Materials and Structures Technology*, F.-K. Chang, C. B. Yun and B. F. Spencer, Jr. (eds.), DEStech, Lancaster, Pennsylvania, USA, 504-511.

Ko, J. M., Wang, J. Y., Ni, Y. Q. and Chak, K. K. (2003), "Observation on environmental variability of modal properties of a cable-stayed bridge from one-year monitoring data", *Struct. Health Monitoring 2003*, F.-K. Chang (ed.), DEStech, Lancaster, Pennsylvania, USA, 467-474.

Link, M., Weiland, M. and Yu, F. (2002), "Modal analysis of railway bridge hangers using artificial and ambient excitation", *J. De Physique IV*, **12**, 101-110.

Ljung, L. (1999), *System Identification: Theory for the User*, 2nd edition, Prentice-Hall, Upper Saddle River, New Jersey, USA.

Lloyd, G. M., Wang, M. L. and Singh, V. (2000), "Observed variations of mode frequencies of a prestressed concrete bridge with temperature", *Proceedings of the 14th Engineering Mechanics Conference*, J. L. Tassoulas (ed.), ASCE, Reston, Virginia, USA (CD-ROM).

Mackay, D. J. C. (1992), "Bayesian interpolation", *Neural Computation*, **4**, 415-447.
Mahmoud, M., Abe, M. and Fujino, Y. (2001), "Analysis of suspension bridge by ambient vibration measurement using time domain method and its application to health monitoring", *Proceedings of the 19th International Modal Analytical Conference*, SEM, Bethel, Connecticut, USA, 504-510.
Morgan, N. and Bourlard, H. (1990), "Generalization and parameter estimation in feedforward nets: some experiments", *Advances in Neural Information Processing System II*, D. S. Touretzky (ed.), Morgan Kaufmann Publishers, San Francisco, California, USA, 630-637.
Ni, Y. Q., Fan, K. Q., Zheng, G. and Ko, J. M. (2005), "Automatic modal identification and variability in measured modal vectors of a cable-stayed bridge", *Struct. Eng. Mech.*, **19**, 123-139.
Ni, Y. Q., Zhou, H. F. and Ko, J. M. (2007), "Generalizing neural networks for characterizing the modal variability: a comparison of alternative approaches", *Research Report*, Department of Civil and Structural Engineering, The Hong Kong Polytechnic University, Hong Kong.
Olson, S. E., DeSimio, M. P. and Derriso, M. M. (2005), "Structural health monitoring incorporating temperature compensation", *Struct. Health Monitoring 2005*, F.-K. Chang (ed.), DEStech, Lancaster, Pennsylvania, USA, 1635-1642.
Pan, T. C., Brownjohn, J. M. W. and You, X. T. (2004), "Correlating measured and simulated dynamic responses of a tall building to long-distance earthquakes", *Earthq. Eng. Struct. Dyn.*, **33**, 611-632.
Peeters, B. and De Roeck, G. (2001), "One-year monitoring of the Z24-Bridge: Environmental effects versus damage events", *Earthq. Eng. Struct. Dyn.*, **30**, 149-171.
Rencher, A. C. (2002), *Methods of Multivariate Analysis*, 2nd edition, Wiley, New York, USA.
Roberts, G. P. and Pearson, A. J. (1996), "Dynamic monitoring as a tool for long span bridges", *Bridge Management 3: Inspection, Maintenance, Assessment and Repair*, J. E. Harding, G. E. R. Parke and M. J. Ryall (eds.), E&FN Spon, London, UK, 704-711.
Rohrmann, R. G., Baessler, M., Said, S., Schmid, W. and Ruecker, W. F. (2000), "Structural causes of temperature affected modal data of civil structures obtained by long time monitoring", *Proceedings of the 18th International Modal Analytical Conference*, SEM, Bethel, Connecticut, USA, 1-7.
Sohn H. (2007), "Effects of environmental and operational variability on structural health monitoring", *Philosophical Transactions of the Royal Society A – Mathematical Physical and Engineering Sciences*, **365**, 539-560.
Sohn, H., Dzwonczyk, M., Straser, E. G., Kiremidjian, A. S., Law, K. H. and Meng, T. (1999), "An experimental study of temperature effect on modal parameters of the Alamosa Canyon Bridge", *Earthq. Eng. Struct. Dyn.*, **28**, 879-897.
Wenzel, H., Veit, R. and Tanaka, H. (2005), "Damage detection after condition compensation in frequency analyses", *Struct. Health Monitoring 2005*, F.-K. Chang (ed.), DEStech, Lancaster, Pennsylvania, USA, 627-633.
Wong, K. Y. (2004), "Instrumentation and health monitoring of cable-supported bridges", *Struct. Control Health Monitoring*, **11**, 91-124.
Xia, Y., Hao, H., Zanardo, G. and Deeks, A. (2006), "Long term vibration monitoring of an RC slab: temperature and humidity effect", *Eng. Struct.*, **28**, 441-452.
Yang, Y. and Zhang, Q. (1997), "A hierarchical analysis for rock engineering using artificial neural networks", *Rock Mech. Rock Eng.*, **30**, 207-222.
Zhang, Q. W., Fan, L. C. and Yuan, W. C. (2002), "Traffic-induced variability in dynamic properties of cable-stayed bridge", *Earthq. Eng. Struct. Dyn.*, **31**, 2015-2021.
Zhou, H. F., Ni, Y. Q. and Ko, J. M. (2007), "Eliminating temperature effect in structural damage alarming using auto-associative neural networks", *Structural Health Monitoring 2007: Quantification, Validation, and Implementation,* F.-K. Chang (ed.), DEStech Publications, Lancaster, Pennsylvania, USA, 539-548.

CC